Fingerprinting-Based Indoor Localization with Commercial MMWave WiFi: NLOS Propagation

Wang, Pu; Koike-Akino, Toshiaki; Orlik, Philip V.

Abstract

In addition to coarse-grained received signal strength indicator (RSSI) measurements and fine-grained channel state information (CSI), a mid-grained channel measurement — spatial beam signal-to-noise ratios (SNRs) — that are inherently available during the millimeter wave (mmWave) beam training as defined in mmWave fifth-generation (5G) and IEEE 802.11ad/ay standards, were recently utilized for fingerprintingbased indoor localization. In this paper, we extend the beam SNR fingerprinting-based indoor localization to more challenging scenarios in non-line-of-sight (NLOS) propagation. Particularly, multi-channel beam covariance matrix (BCM) images are used as the fingerprinting signature and fed into a beam covariance learning (BCL) network to identify the position and estimate the coordinate. Using our in-house testbed with commercial off-theshelf (COTS) 60-GHz WiFi routers, real-world mmWave BCMs are fingerprinted in several NLOS locations-of-interest in an enclosed L-shape conference room. Given a fingerprinting gridsize of 30 cm, preliminary performance evaluation shows the position classification accuracy can be above 90% using classical classification methods and a coordinate estimation error around 11 cm with the BCL approach.

IEEE Global Communications Conference (GLOBECOM)

Fingerprinting-Based Indoor Localization with Commercial MMWave WiFi: NLOS Propagation

Pu Wang, Toshiaki Koike-Akino, and Philip V. Orlik

Mitsubishi Electric Research Laboratories (MERL), Cambridge, MA 02139, USA

Abstract—In addition to coarse-grained received signal strength indicator (RSSI) measurements and fine-grained channel state information (CSI), a mid-grained channel measurement — spatial beam signal-to-noise ratios (SNRs) — that are inherently available during the millimeter wave (mmWave) beam training as defined in mmWave fifth-generation (5G) and IEEE 802.11ad/ay standards, were recently utilized for fingerprinting-based indoor localization. In this paper, we extend the beam SNR fingerprinting-based indoor localization to more challenging scenarios in non-line-of-sight (NLOS) propagation. Particularly, multi-channel beam covariance matrix (BCM) images are used as the fingerprinting signature and fed into a beam covariance learning (BCL) network to identify the position and estimate the coordinate. Using our in-house testbed with commercial off-the-shelf (COTS) 60-GHz WiFi routers, real-world mmWave BCMs are fingerprinted in several NLOS locations-of-interest in an enclosed L-shape conference room. Given a fingerprinting grid-size of 30 cm, preliminary performance evaluation shows the position classification accuracy can be above 90% using classical classification methods and a coordinate estimation error around 11 cm with the BCL approach.

Index Terms—Millimeter wave, indoor localization, 5G, WiFi, beam training, beam SNR, NLOS propagation.

I. INTRODUCTION

WiFi-based indoor localization has received long attraction over the past two decades. Among all frameworks, *fingerprinting-based* methods provide an efficient solution for online localization with low computational complexity [1]. On the other hand, it requires enormous time and resources to construct an offline database with chosen fingerprinting features at locations-of-interest to enable fast online localization. In the following, we provide a brief review of two mainstream channel measurements and one emerging millimeter wave (mmWave) channel measurement for the fingerprinting-based indoor localization:

A. Coarse-Grained Received Signal Strength Indicator (RSSI)

Early WiFi-based indoor localization systems have used received signal strength indicator (RSSI) measurements to estimate indoor location in a direct localization fashion [2], [3]. For fingerprinting-based methods, RSSI has been used directly as fingerprinting data in systems such as Radar [1], Compass [4], and Horus [5]. Classical machine learning methods such as the k-nearest neighbor (kNN) and support vector machine (SVM) have been applied to RSSI fingerprinting measurements [6], [7]. Leveraging modern machine learning frameworks such as discriminant-adaptive neural network [8],

robust extreme learning machine [9], and multi-layer neural networks [10], RSSI fingerprinting-based indoor localization methods have shown improved localization performance over classical machine learning approaches. More recently, [11] proposed to apply recurrent neural networks (RNNs) to further utilize the trajectory information.

B. Fine-Grained Channel State Information (CSI)

At low frequency bands, CSI measurements can be accessed from commercial off-the-shelf (COTS) 802.11n/ac/h devices. These measurements are complex-valued channel measurements across subcarriers at 2.4 or 5 GHz bands [12]–[15]. With richer channel information, a larger amount of CSI measurements from fingerprinted locations can be trained by advanced deep learning architectures, e.g., ConFi [16], autoencoder [17] and direct regression methods [18], to learn the mapping from the CSI to locations.

At mmWave bands (e.g, 28-GHz and 60 GHz), the use of CSI measurements for fingerprinting is much less reported due to the cost of a dedicated mmWave platform or limited access to CSI measurements from COTS mmWave WiFi devices. RSSI and angle-of-arrival from multiple access points (APs) are fingerprinted and then used to estimate location using the weighted nearest neighbor algorithm [19]. A two-dimensional power delay profile (PDP) over multiple beampatterns is used as fingerprints at 28 GHz band for outdoor localization [20]. However, this concept was verified only using ray-tracing simulated datasets. More recently, [21] reported a field study using real-world 28-GHz channel frequency responses over a bandwidth of 500 MHz for the fingerprinting-based outdoor localization.

C. Mid-Grained Beam SNR

The RSSI feature suffers from the measurement instability and coarse granularity of the channel information, leading to limited accuracy for localization. The CSI measurement is more fine-grained but requires access to physical-layer interfaces and high computational power to process a large amount of subcarrier data. These limitations motivate a recent introduction of mid-grained intermediate channel measurements — beam SNRs — which are more informative (e.g., in the spatial domain) than the RSSI and easier to access than the lower-level CSI [22]–[24]. The spatial beam SNRs can be accessed during the beam training phase for the fifth-generation (5G) and IEEE 802.11ad/ay standards operating

at the mmWave bands and, hence, introduces no overhead. Comprehensive performance evaluation using real-world beam SNRs from COTS 802.11ad routers confirms the effectiveness of the beam SNR-based indoor localization.

D. Extension to NLOS Scenarios

In this paper, we extend our previous study on beam SNR-based fingerprinting localization to more challenging scenarios at non-line-of-sight (NLOS) propagation. This is motivated by the fact that the mmWave link in the NLOS scenario may be subject to larger path losses and greater probabilities of outage than the LoS scenario. It is thus of interest to investigate the fingerprinting-based NLOS indoor localization.

Compared with our previous use of beam SNR measurements directly as fingerprinting signatures, we propose to fingerprint the mmWave beam covariance matrix (BCM) for the following reasons:

- The use of BCM can overcome measurement fluctuations over time and possibly mitigate interference due to subtle environmental changes, e.g., people and furniture moving. This is particularly critical in the NLOS propagation scenario since mmWave NLOS links are considerably weaker than those in an LoS propagation scenario and are more prone to environmental perturbation.
- Frequent beam training is required to establish mmWave communication links and, in turn, provides sufficient beam SNR measurements over a tight time interval (e.g., milli-seconds to locate moving objects in most indoor environments) to construct BCM fingerprints at locations-of-interest.
- A direct benefit of using the BCM is that one can stack the BCMs from multiple APs as a multi-channel input image and leverage advanced deep convolution neural network (CNN) architecture, e.g., residual network (ResNet) [25], to recognize location-specific features from the BCM images.

To verify the above claims, we use an experimental platform consisting of COTS 60-GHz WiFi routers that are compliant the 802.11ad standards and fingerprint the BCMs over 10 NLOS locations in an enclosed L-shape conference room. The BCM images are then used by classical classification methods for positioning and by a ResNet-based beam covariance learning (BCL) for direct coordinate estimation.

II. DATA COLLECTION SYSTEM

A. Hardware

We use TP-Link Talon AD7200 routers to build our in-house experimental system. Complying with IEEE 802.11ad standards, this router implements Qualcomm QCA9500 transceiver that supports a single stream communication in 60 GHz range using analog beamforming over 32-element planar array. To search for desired directions, a series of pre-defined beam-patterns or sectors are used by APs to send beacons to potential clients which are in a listening mode with a quasi-omnidirectional beampattern. Then, clients send a series of
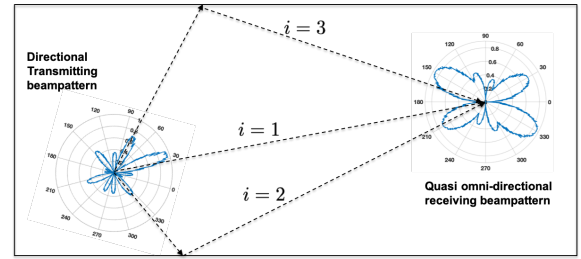

Fig. 1: Illustration of beam SNR measurements as a function of transmitting and receiving beampatterns.

beampatterns while the APs are in a listening mode. After beam training, the link can be established by choosing the pair of beampatterns between the AP and clients. Such beam training is periodically repeated and the beam sectors are updated to adapt to the environmental changes. It is noted that the beampatterns reported in [26], [27] exhibit irregular shapes due to hardware imperfections and housing at 60 GHz.

B. Beam SNR

When directional beampatterns are used, beam SNRs are collected by 802.11ad devices as a measure of beam quality. For a given pair of transmitting and receiving beampatterns, corresponding beam SNR can be defined as[1]

$$h_m = \text{BeamSNR}_m = \frac{1}{\sigma^2} \sum_{i=1}^{I} \gamma_m(\theta_i)\zeta_m(\psi_i)P_i, \quad (1)$$

where m is the index of beampattern, I is the total number of paths, θ_i and ψ_i are the transmitting and receiving azimuth angles for the ith path, respectively, P_i is the signal power at the ith path, $\gamma_m(\theta_i)$ and $\zeta_m(\psi_i)$ are the transmitting and receiving beampattern gains at the ith path for the mth beampattern, respectively, and σ^2 is the noise variance. Fig. 1 shows an example of $I = 3$ paths between the transmitting side that probes the spatial domain using a beampattern ($m = 24$) and the receiving side which is in a listening mode.

To access the raw beam SNR measurements at Talon AD7200 routers, we followed the work in [26]–[28] and used the open-source software package in [29]. Particularly, we used the Nexmon firmware patching framework [30], which enables the development of binary firmware extensions in C.

C. Beam Covariance Matrix (BCM)

Fig. 2 shows 20 fingerprinted BCM images that are randomly selected from the fingerprinting dataset. Corresponding location labels correspond to one of 10 NLOS fingerprinted locations in Fig. 5. Each BCM is of the size of 36×36 due to the use of 36 beampatterns for beam training. It is seen that the BCM images show repeatable and stable patterns for the same NLOS locations (e.g., 1B, 2A, and 3A), and distinct features over different locations.

---

[1]For simplicity and illustration in Fig. 1, we only consider the definition of beam SNR in the azimuth domain. In practice, beam SNRs are a function of the beam pattern over the azimuth and elevation angles.
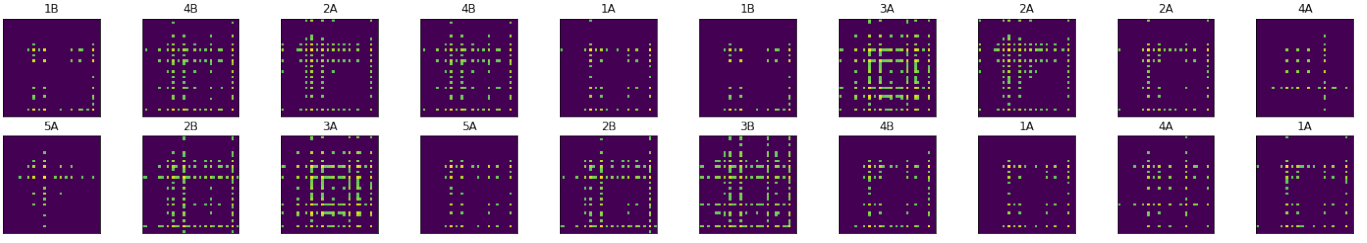
Fig. 2: Plots of 20 randomly selected beam covariance matrix (BCM) images for 10 NLOS locations in Fig. 5. Brighter pixels denote larger elements of the BCM of (3). Consistent patterns can be observed for most locations, except that the patterns of 4A and 5A show larger variations due to those BCM pixels having similar sample covariance to the threshold λ.
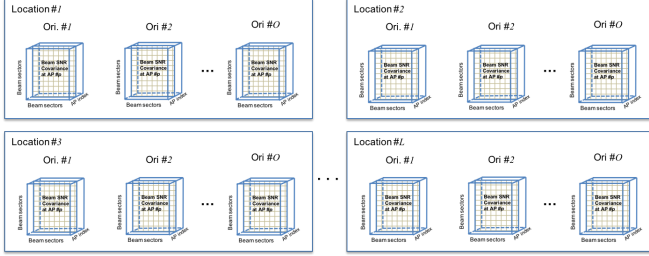

Fig. 3: Offline BCM fingerprinting dataset at different locations and orientations.

III. INDOOR LOCALIZATION BY MMWAVE BCM

In the following, we introduce the proposed BCL approach for the mmWave fingerprinting-based indoor localization.

A. Offline Fingerprinting

We first group beam SNRs from all beam sectors as $\mathbf{h} = [h_1, h_2, \ldots, h_M]^T$ where $M = 36$ is the number of beam-patterns used for beam training. For a given location and orientation, R beam SNR measurements, $\mathbf{h}_1(l, o), \ldots, \mathbf{h}_R(l, o)$, are collected to construct the offline fingerprinting dataset, where l and o are the indices for the location and orientation, respectively. To compute the BCM, we follow the tradition to first normalize the beam SNR measurements as $\tilde{\mathbf{h}}_r$, apply the optional standardization operation, and compute the sample covariance matrix over an index set $\mathbb{S}_i$:

$$\mathbf{C}_i = \frac{1}{N_s} \sum_{r \in \mathbb{S}_i} \tilde{\mathbf{h}}_r \tilde{\mathbf{h}}_r^T, \quad i \in \{1, 2, \cdots, N_R\}, \quad (2)$$

where $\mathbb{S}_i$ is the ith subset of N_s time indices (sequentially or randomly) selected from the R fingerprinting snapshots. For the deep learning-based localization methods, one can augment the offline training datasets by randomly shuffling the N_s time indices. To further enhance the unique features from the sample covariance matrix, we keep only significant covariances that are above a certain threshold λ and ignore insignificant covariances due to its instability over time:

$$\mathbf{B}_i = \mathbf{C}_i \odot \mathbb{1}_{\mathbf{C}_i \geq \lambda}, \quad (3)$$

where $\odot$ denotes the element-wise product and $\mathbb{1}$ is an element-wise indicator function. The above process repeats

over different locations and orientations for fingerprinting $\mathbf{B}_i(l, o)$. When multiple APs are available, we stack each BCM from one AP across an image channel as $\tilde{\mathbf{B}}_i(l, o) = \{\mathbf{B}_i^p(l, o)\}_{p=1}^P$ with P denoting the number of APs. As shown in Fig. 3, each 3D datacube is a P-channel BCM image $\tilde{\mathbf{B}}_i(l, o)$ for location l and orientation i. Each pair of location and orientation can have N_R such BCM images.

B. Online Localization by Beam Covariance Learning (BCL)

When new fingerprinting measurements from an unknown location are available, the problem of interest is to identify its location and/or orientation and estimate its coordinate. In the following, we introduce a BCL approach which learns location-specific patterns from the multi-channel BCM images using a deep convolutional ResNet with a multi-purpose output layer for: 1) location-only classification; 2) simultaneous location-and-orientation classification; and 3) direct coordinate estimation. For the classification, we also consider classical machine learning methods such as the kNN and SVM.

The proposed BCL architecture for the fingerprinting-based indoor localization is shown in Fig. 4 which is based on the ResNet [25] having a different output layer for each task. It first feeds the P-channel BCM images from multiple APs to the input of the neural network. The input layer is implemented with a convolution layer with a kernel size of 3×3 followed by a batch normalization (BN) layer, rectified linear unit (ReLU) activation, and a max pooling to downsize the BCM images to a 4-channel feature map $\mathbf{y}_0$ with a dimension of 18×18.

Then, the output $\mathbf{y}_0$ of the input layer is fed into N_d consecutive residual blocks, where a shortcut connection is used to jump from the input to the output of each residual block to learn residual gradient for improved training stability. For the ℓth residual block, its output $\mathbf{y}_\ell$ is given as

$$\mathbf{y}_\ell = f_\ell(\mathbf{y}_{\ell-1}, \boldsymbol{\theta}_\ell) + \mathbf{y}_{\ell-1}, \quad \ell = 1, 2, \ldots, N_d, \quad (4)$$

where f_ℓ is the nonlinear mapping with weights $\boldsymbol{\theta}_\ell$ implemented by 2D convolution filters and N_d is the number of residual blocks.

For the residual block architecture, the form of f_ℓ can be flexible in terms of the configuration of convolution kernels, the number of convolution layers, the use of bottleneck layers
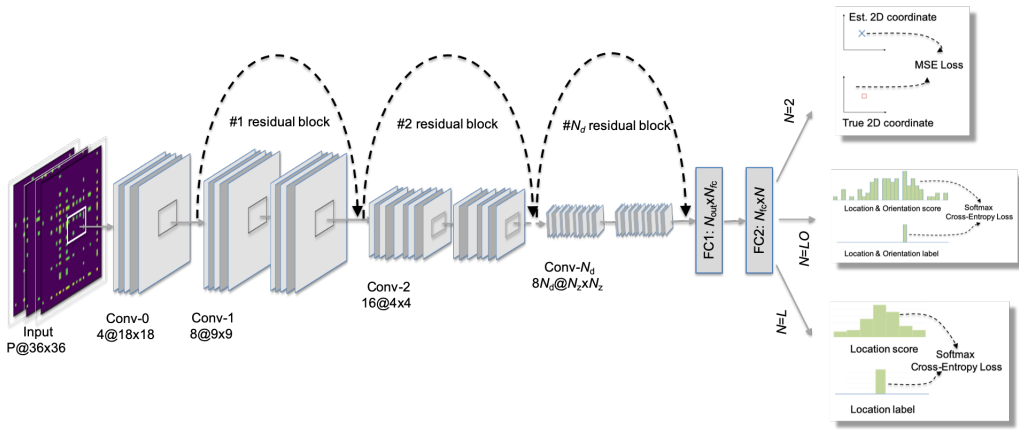
Fig. 4: Proposed beam covariance learning (BCL) approach for the fingerprinting-based indoor localization. The architecture follows a ResNet architecture for multiple purposes: 1) location-only identification; 2) simultaneous location-and-orientation classification; and 3) direct coordinate estimation.

for dimension reduction, activation functions, and regularization formats. In Fig. 4, we employed a stride of 2 at the first convolution layer of each residual block to first downsize the input to each residual bloc and used the BN and ReLU layers after the convolution layer. Due to the downsizing operation, the shortcut connection (denoted as dash lines in Fig. 4) was implemented by a projection operation with a stride of 2.

Finally, for the output layer, we use multiple fully-connected layers to generate an output vector with a dimension of N, where N is determined by the objective: 1) $N = L$ for the location-only classification; 2) $N = LO$ for the simultaneous location-and-orientation classification; and 3) $N = 2$ for the 2D coordinate estimation. For the first two classification tasks, the softmax cross-entropy loss is used as the cost function, while the mean-square error (MSE) is used for the coordinate estimation.

IV. PERFORMANCE EVALUATION

In this section, we present our results for the beam SNR fingerprinting-based localization method using the beam SNR covariance matrix and compare the localization performance with respect to the RSSI-like single SNR fingerprinting-based localization method.

A. In-House NLOS Indoor Experiment Data

The testbed consists of two 802.11ad devices, one serving as AP and one serving as the client. The testbed is deployed in an L-shape conference room as shown in Fig. 5. Furniture including chairs, tables, and desktops are present in the conference room. One AP, denoted as red triangles, is fixed near Entrance 2 with a fixed orientation. To fingerprint the location, we position the client at one of 10 locations-of-interest (marked by crosses in Fig. 5) near Entrance 1 with no obvious LoS links to the AP. For each location, we collected
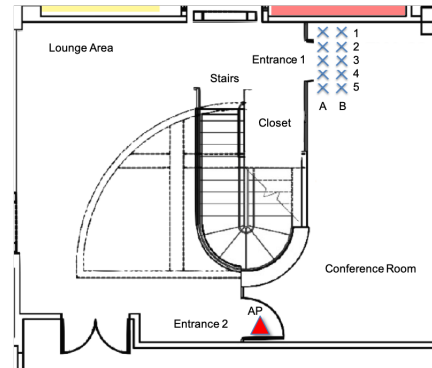

Fig. 5: Experimental setup in an L-shape conference room with 10 NLOS locations-of-interest (denoted by crosses). The AP is denoted as the red triangle.

beam SNR measurements for $O = 1$ orientation[2]. Samples of the BCM images collected from these 10 fingerprinted locations are shown in Fig. 2.

B. Location Classification

For the location classification, we use the confusion matrix as a performance metric:

$$\mathbf{C}(i,j) = \frac{1}{T_i} \sum_{t=1}^{T_i} \mathbb{1}[\hat{l}(\tilde{\mathbf{h}}_t(j)) = i], \tag{5}$$

where i and j are indices, respectively, for the estimated and true locations/orientations, T_i is the number of sample batches in the test dataset, and $\hat{l}(\tilde{\mathbf{h}}_t(j))$ is the location estimate with the tth batch from the test data collected at the jth location.

[2]It is preferred to collect more measurements with more $O > 1$ orientations and multiple data sessions well separated over time, as we previously did in the LOS scenario [24]. However, due to the impact of COVID-19 and limited access to the office, we were only able to collect measurements for $O = 1$ orientation with only one data session which later we randomly split into the training, validation, and test samples.
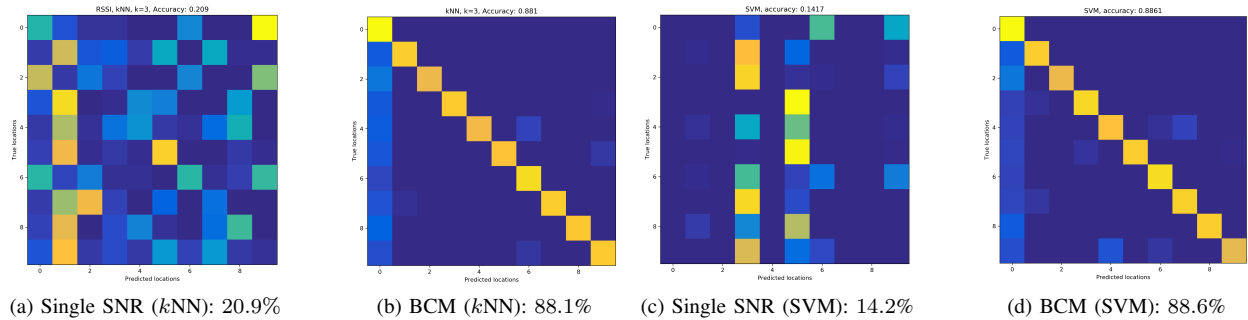
(a) Single SNR (*k*NN): 20.9%   (b) BCM (*k*NN): 88.1%   (c) Single SNR (SVM): 14.2%   (d) BCM (SVM): 88.6%

Fig. 6: Comparison between the RSSI-like single SNR and BCM fingerprinting methods in the NLOS scenario.

(a) *k*NN: median 24.64 cm, RMSE 25.72 cm   (b) GPR: median 22.66 cm, RMSE 29.66 cm   (c) BCL: median 10.38 cm, RMSE 11.03 cm
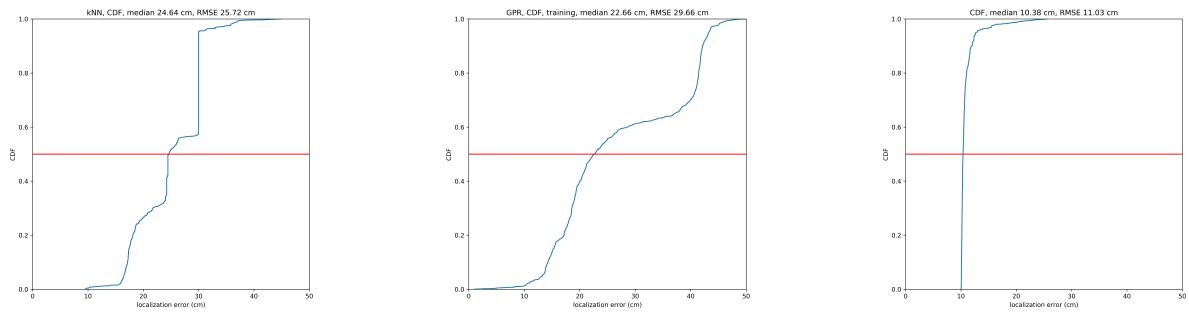
Fig. 7: CDF curves of localization error for the *k*NN, GPR and the proposed BCL coordinate estimation methods.

Fig. 6 compares the confusion matrices between the RSSI-like single SNR fingerprinting and the BCM fingerprinting. The RSSI-like measurements are extracted from one beam sector from the beam SNR dataset which yields the largest average SNR. In this case, the beam SNR from the 16th beam sector is used to construct the training and test dataset for the RSSI-like fingerprinting. Fig. 6 includes two classical classification methods: 1) the *k*NN and 2) SVM. It is easy to see that the conventional RSSI-like method fails to detect the position with one AP in the NLOS scenario. It is worth noting that using multiple APs can improve the positioning performance for the single SNR fingerprinting method. In [24], the single SNR fingerprinting method can yield a classification accuracy around 50% with 3 APs in an LoS scenario. With less APs in a more challenging NLOS scenario, it is not surprising to see the classification accuracy of the RSSI-like fingerprinting method drops to the level around 20%.

On the other hand, by using the BCM images as fingerprinting signatures, the probability of correct classification improves to 88.1% for the *k*NN method with $k = 3$ and 88.6% for the SVM method. This is slightly worse than our previous study in the LoS scenario; see more details in Table 5 of [24].

To evaluate the impact of classification methods, we also evaluate other classical machine learning methods including the linear discriminant analysis (LDA), quadratic discriminant analysis (QDA) and decision tree (DT). The results are shown

in Table I. Overall, we observe that 1) the classification using the proposed BCM significantly improves the positioning accuracy over that using the single SNR; 2) all classification methods except the QDA and DT show similar performance with a classification accuracy above 80% with a threshold $\lambda = 0.5$ and a high 90.4% with a threshold $\lambda = 0.75$; and 3) a proper threshold ($\lambda = 0.75$) in (3) can preserve useful signatures while removing unstable fluctuating features and improve the classification accuracy.

C. Coordinate Estimation

To evaluate the performance of coordinate estimation, we divide the 10 locations into the training, validation and testing locations in Fig. 5; specifically, the training set includes [1A, 1B, 2B, 3A, 5A, 5B], the validation set has 2 locations at [2A, 4B], and the rest 2 locations at [3B, 4A] are used for testing.

TABLE I: Impact of Classification Methods

	Location Identification Accuracy		
	RSSI	BCM ($\lambda = 0.5$)	BCM ($\lambda = 0.75$)
LDA	10.4%	**87.4%**	**90.4%**
QDA	8.7%	62.5%	73.7%
SVM	14.2%	81.1%	88.6%
DT	**25.1%**	73.0%	78.3%
1NN	17.2%	81.2%	88.1%
3NN	20.9%	81.1%	88.1%

For comparison, we employ the weighted kNN method and the Gaussian process regression (GPR) method for the same datasets. Fig. 7 shows the cumulative distribution function (CDF) of the localization errors at the two testing locations. For the weighted kNN method in Fig. 7(a), the median location error is about 22.64 cm with a root MSE (RMSE) of 25.72 cm. With the radial-basis function kernel, the GPR method slightly improves the median location error to 22.66 cm, while the RMSE increases to 29.66 cm. For the BCL method, we train the proposed neural network with the BCM from the 6 training locations, calculate the validation errors using the BCM images from the two validation locations, and identify the best trained model from the validation error. Fig. 7(c) shows the CDF of the localization errors for the proposed method, which gives a median location error of 10.38 cm and an RMSE of 11.03 cm, which are grater than 2.5-fold improvement over classical machine learning methods.

V. Conclusions

This paper extends our previous study on the mmWave indoor localization using beam SNR measurements towards challenging scenarios at the NLOS propagation. By collecting real-world beam SNRs in an L-shape conference room and fingerprinting 10 locations with a grid size of 30 cm, we demonstrated that the classification accuracy can improve from a level of 20% using the RSSI-like measurement to higher than 80% accuracy using the beam covariance matrix. In addition, greater-than 2.5 improvement for coordinate estimation was verified for our in-house experiments of NLOS environment.

References

[1] P. Bahl and V. N. Padmanabhan, "RADAR: an in-building RF-based user location and tracking system," in *INFOCOM*, March 2000.

[2] X. Li, "RSS-based location estimation with unknown pathloss model," *IEEE Transactions on Wireless Communications*, vol. 5, no. 12, pp. 3626–3633, December 2006.

[3] S. Mazuelas et. al., "Robust indoor positioning provided by real-time RSSI values in unmodified WLAN networks," *IEEE Journal of Selected Topics in Signal Processing*, vol. 3, no. 5, pp. 821–831, Oct 2009.

[4] T. King, S. Kopf, T. Haenselmann, C. Lubberger, and W. Effelsberg, "COMPASS: A probabilistic indoor positioning system based on 802.11 and digital compasses," in *WiNTECH*, Sep. 2006.

[5] M. Youssef and A. Agrawala, "The horus location determination system," *Wirel. Netw.*, vol. 14, no. 3, pp. 357–374, June 2008.

[6] M. Brunato and R. Battiti, "Statistical learning theory for location fingerprinting in wireless LANs," *Computer Networks*, vol. 47, no. 6, pp. 825 – 845, 2005.

[7] D. Li, B. Zhang, Z. Yao, and C. Li, "A feature scaling based k-nearest neighbor algorithm for indoor positioning system," in *2014 IEEE Global Communications Conference*, Dec 2014, pp. 436–441.

[8] S. Fang and T. Lin, "Indoor location system based on discriminant-adaptive neural network in IEEE 802.11 environments," *IEEE Transactions on Neural Networks*, vol. 19, no. 11, pp. 1973–1978, Nov 2008.

[9] X. Lu, H. Zou, H. Zhou, L. Xie, and G. Huang, "Robust extreme learning machine with its application to indoor positioning," *IEEE Transactions on Cybernetics*, vol. 46, no. 1, pp. 194–205, Jan 2016.

[10] H. Dai, W. Ying, and J. Xu, "Multi-layer neural network for received signal strength-based indoor localisation," *IET Communications*, vol. 10, no. 6, pp. 717–723, 2016.

[11] M. T. Hoang, B. Yuen, X. Dong, T. Lu, R. Westendorp, and K. Reddy, "Recurrent neural networks for accurate RSSI indoor localization," *IEEE Internet of Things Journal*, vol. 6, no. 6, pp. 10639–10651, Dec 2019.

[12] C. Chen et. al., "Achieving centimeter-accuracy indoor localization on WiFi platforms: A multi-antenna approach," *IEEE Internet of Things Journal*, vol. 4, no. 1, pp. 122–134, Feb 2017.

[13] X. Wang, L. Gao, S. Mao, and S. Pandey, "CSI-based fingerprinting for indoor localization: A deep learning approach," *IEEE Transactions on Vehicular Technology*, vol. 66, no. 1, pp. 763–776, Jan 2017.

[14] X. Wang, L. Gao, and S. Mao, "Biloc: Bi-modal deep learning for indoor localization with commodity 5GHz WiFi," *IEEE Access*, vol. 5, pp. 4209–4220, 2017.

[15] C. Hsieh, J. Chen, and B. Nien, "Deep learning-based indoor localization using received signal strength and channel state information," *IEEE Access*, vol. 7, pp. 33256–33267, 2019.

[16] H. Chen, Y. Zhang, W. Li, X. Tao, and P. Zhang, "ConFi: Convolutional neural networks based indoor Wi-Fi localization using channel state information," *IEEE Access*, vol. 5, pp. 18066–18074, 2017.

[17] X. Wang, L. Gao, and S. Mao, "CSI phase fingerprinting for indoor localization with a deep learning approach," *IEEE Internet of Things Journal*, vol. 3, no. 6, pp. 1113–1123, Dec 2016.

[18] C. Xiang, S. Zhang, S. Xu, X. Chen, S. Cao, G. C. Alexandropoulos, and V. K. N. Lau, "Robust sub-meter level indoor localization with a single WiFi access point?regression versus classification," *IEEE Access*, vol. 7, pp. 146309–146321, 2019.

[19] Z. Wei, Y. Zhao, X. Liu, and Z. Feng, "DoA-LF: A location fingerprint positioning algorithm with millimeter-wave," *IEEE Access*, vol. 5, pp. 22678–22688, 2017.

[20] J. Gante, G. Falcão, and L. Sousa, "Beamformed fingerprint learning for accurate millimeter wave positioning," in *2018 VTC Fall*, Aug 2018.

[21] H. Sun, P. Wang, M. Pajovic, T. Koike-Akino, and P.V. Orlik, "Fingerprinting-based outdoor localization with 28-GHz channel measurement: A field study," in *IEEE SPAWC*, May 2020.

[22] M. Pajovic, P. Wang, T. Koike-Akino, H. Sun, and P. V. Orlik, "Fingerprinting-based indoor localization with commercial MMWave WiFi–Part I: RSS and Beam Indices," in *2019 IEEE Global Communications Conference (GLOBECOM)*, Dec. 2019.

[23] P. Wang, M. Pajovic, T. Koike-Akino, H. Sun, and P.V. Orlik, "Fingerprinting-based indoor localization with commercial mmwave WiFi–Part II: Spatial beam SNRs," in *2019 IEEE Global Communications Conference (GLOBECOM)*, Dec 2019.

[24] T. Koike-Akino, P. Wang, M. Pajovic, H. Sun, and P.V. Orlik, "Fingerprinting-based indoor localization with commercial MMWave WiFi: A deep learning approach," *IEEE Access*, pp. 1–1, 2020.

[25] K. He, X. Zhang, S. Ren, and J. Sun, "Deep residual learning for image recognition," in *2016 IEEE Conference on Computer Vision and Pattern Recognition (CVPR)*, June 2016, pp. 770–778.

[26] D. Steinmetzer, D. Wegemer, M. Schulz, J. Widmer, and M. Hollick, "Compressive millimeter-wave sector selection in off-the-shelf IEEE 802.11ad devices," in *CoNEXT 2017*, December 2017.

[27] G. Bielsa et. al., "Indoor localization using commercial off-the-shelf 60 GHz access points," in *IEEE INFOCOM 2018*, April 2018, pp. 2384–2392.

[28] S. K. Saha et. al., "Fast and infuriating: Performance and pitfalls of 60 GHz WLANs based on consumer-grade hardware," in *SECON'18*, June 2018.

[29] D. Steinmetzer, D. Wegemer, and M. Hollick, "Talon tools: The framework for practical IEEE 802.11ad research," in *Available: https://seemoo.de/talon-tools/*, 2018.

[30] M. Schulz, D. Wegemer, and M. Hollick, "Nexmon: The c-based firmware patching framework," in *Available: https://nexmon.org*, 2017.